Electronic Supplementary Material (ESI) for Nanoscale Horizons.

Electronic Supplementary Material (ESI)

Polarization Dependent Asymmetric Transmission Using Bifacial Metasurface

*Jangwoon Sung, Gun-Yeal Lee, Chulsoo Choi, Jongwoo Hong and Byoungho Lee**

School of Electrical and Computer Engineering and Inter-University Semiconductor Research Center, Seoul National University, Gwanak-Gu Gwanakro 1, Seoul 08826, Republic of Korea

Part 1. Two independent phase retardation of birefringent meta-atom

Here we demonstrate analytically how the two distinct and independent phase control is possible with arbitrary orthogonal polarization pairs. Since the linear and circularly polarization pair is intuitive and well-known by the several papers, the general case of elliptical polarization basis is explored here. We consider the case of generalized elliptical polarization pair, which are expressed as follows through the Jones matrix,

$$\mathbf{E}_{\phi}=(\left|E_{\phi 1}\right\rangle,\left|E_{\phi 2}\right\rangle)=\left(\frac{1}{\sqrt{2}}\begin{bmatrix}1\\ e^{i\phi}\end{bmatrix},\frac{1}{\sqrt{2}}\begin{bmatrix}-1\\ e^{i\phi}\end{bmatrix}\right), \quad \text{* MERGEFORMAT (S1)}$$

where $\mathbf{E}_{\phi}$ denotes the basis matrix of electric field direction of input light that is orthogonal to each other component, and ϕ is the phase difference between x- and y-directional electric field at incident light. Considering that the phase retardation in linear polarization basis of meta-atoms and rotation angle in xy-plane is freely adjustable, Jones matrix of meta-atom that is equivalent to scattering effect can be written as

$$\mathbf{J}=\mathbf{R}(\theta)\begin{pmatrix}e^{j\phi_{xx}} & 0\\ 0 & e^{j\phi_{yy}}\end{pmatrix}\mathbf{R}(-\theta), \qquad \text{* MERGEFORMAT (S2)}$$

where θ is rotation angle of each meta-atom with respect to x-axis, and $\mathbf{R}$ is well-known 2 by 2 rotation matrix expressed as

$$\mathbf{R}(\theta)=\begin{pmatrix}\cos\theta & -\sin\theta\\ \sin\theta & \cos\theta\end{pmatrix}. \qquad \text{* MERGEFORMAT (S3)}$$

Here, when the incident light is expressed by Equation (S1) and incident onto meta-atom, the scattering matrix expressed by polarization of which the handedness is flipped from incident one can be written as follows,

$$\mathbf{T}_{-\phi\phi}=\mathbf{E}_{-\phi}^{-1}\times\mathbf{J}\times\mathbf{E}_{\phi}=\begin{pmatrix}\left\langle E_{-\phi 1}\middle|E_{\phi 1}\right\rangle & \left\langle E_{-\phi 1}\middle|E_{\phi 2}\right\rangle\\ \left\langle E_{-\phi 2}\middle|E_{\phi 1}\right\rangle & \left\langle E_{-\phi 2}\middle|E_{\phi 2}\right\rangle\end{pmatrix}=\frac{e^{i\phi}}{2}\begin{pmatrix}ae^{i\phi_{xx}}+be^{i\phi_{yy}} & ce^{i\phi_{xx}}-\overline{c}e^{i\phi_{yy}}\\ ce^{i\phi_{xx}}-\overline{c}e^{i\phi_{yy}} & \overline{b}e^{i\phi_{xx}}+\overline{a}e^{i\phi_{yy}}\end{pmatrix} \text{* MERGEFORMA}$$

where a, b, and c are the derived complex coefficients as below,

$$\begin{aligned} a &= \cos\phi + \sin 2\theta - i\cos 2\theta \sin\phi, \\ b &= \cos\phi - \sin 2\theta + i\cos 2\theta \sin\phi, \\ c &= -\cos\phi \cos 2\theta + i\sin\phi. \end{aligned}$$ * MERGEFORMAT (S5)

The upper bar in equation (S4) indicates the conjugate value of corresponded parameter. It is notable that the non-diagonal components have same values. Therefore, considering the energy conservation law, when the absolute values of non-diagonal components in $\mathbf{T}_{-\phi\phi}$ are zero, the absolute values of diagonal components, which are handedness-flipped polarized components from incident light, become the highest value of unity. From equation (S4), the zero absolute value condition of non-diagonal components can be expressed as below,

$$\phi_{yy} - \phi_{xx} = 2\angle c$$ * MERGEFORMAT (S6)

Furthermore, since the phase difference between two diagonal components is also achievable with fine-tuning of $\phi_{xx}+\phi_{yy}$, it is possible to impart two distinct phases for arbitrary polarization pair with linearly birefringent meta-atom.

Part 2. Diffration law of L=2

Here we show how the diffraction is determined at PGM when the critical angle condition is fulfilled. In the main text, only the normal incident condition is considered, but for better understanding of equifrequency contour, let us explain with the condition of m=3 and $\xi<k_0$. As shown in the Fig. S19a, the diffraction is decided by the GSL when the incident angle is not in the critical angle condition. The equifrequency contour of diffraction order shows the beam trajectory of refracted beam, as shown in contour at Fig. S19b. Note that the contour is described according to eq. (3), which is same when n=1 in eq. (4). According to the contour, the fact that the refracted beam of the critical condition when k_{in} is bigger than k_0-ξ cannot be explained by GSL (Figs. S19c-d). This is when the light propagates backward because there is no diffraction channel for light beam to proceed. As mentioned in the main text, with

induced reflection, the light is retarded by propagation phase of each nanopillar again. As a result, the diffraction occurs in reflection with opposite sign of transmission, considering the 2π phase wrap as shown in Fig. S19e. As a result, the diffraction order becomes n=-1 (Fig. S19f). Therefore, the equifrequency of GSL cannot explain the diffraction from induced reflection. In the critical angle condition, diffraction is determined by eq. (4) ($n = 2(L)-3(n)$), and the generated diffraction order n follows the equation (5), which is generalized case of abovementioned example.

Part 3. Device fabrication

The device used in experimental section is fabricated on quartz wafer substrate by standard electron beam lithography process. At first, the silicon oxide of 100 nm and following amorphous silicon of 500 nm is deposited using PECVD (Applied Materials P5000, OEM group) based on SiH_4 and He. Next, a double-layer positive-tone resist PMMA 495K A4 and 950K A2 is successively spun on sample at rotation speed of 3000 rpm, then baked for 3 minutes on 180 degrees Celsius. Nano-patterning is performed with commercial electron beam lithography device (JBX-6300FS, JEOL) at 100 kV condition. Exposed sample is developed using MIBK:IPA 1:3 solution for 90 seconds, then rinsed in IPA and flowing water for 30 and 15 seconds, respectively. Using electron beam evaporator, 30 nm chromium is deposited on that sample to form chromium hard mask for dry etch. Then the sample is soaked in acetone for one minute at room temperature for PMMA layer to be removed. Next, amorphous silicon is etched via ICP-RIE tool to get the final device. Finally, remnant chromium layer is wet etched by commercial chromium etchant.

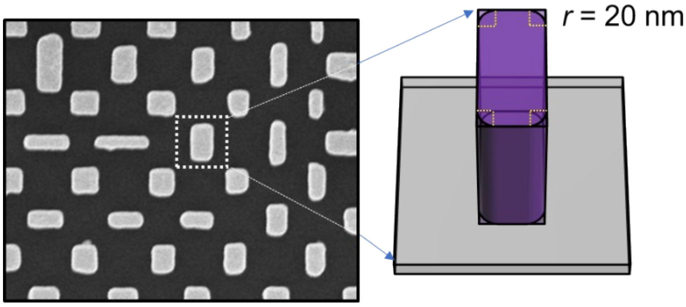

Figure S1. Schematic diagram and SEM captured image showing how the meta-atom is structured and made in simulation and experiment. To minimize the difference between simulation and experiment, the corners of each meta-atom are trimmed into rounded corner.

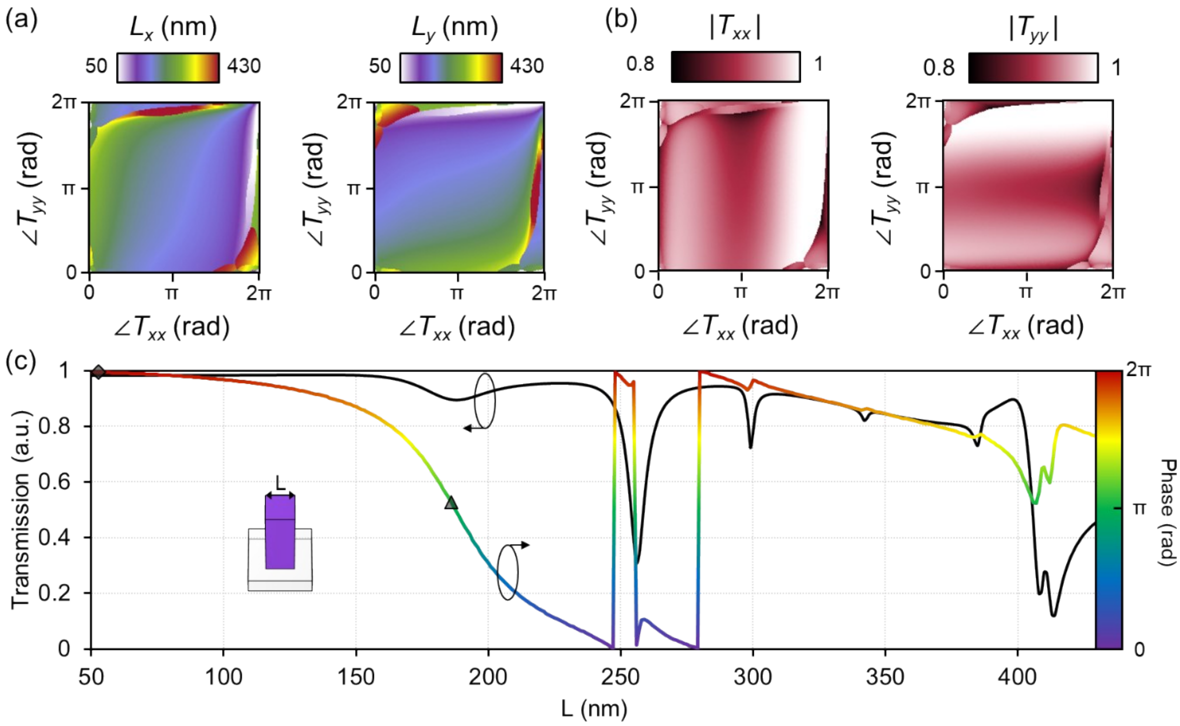

Figure S2. Structural parameter and amplitude data set used in the main text sorted by the desired phase values of T_{xx} and T_{yy}. (a) Colored plot graphs of structural values of L_x and L_y. Coordinate values indicate the lengths of corresponded phase values of T_{xx} and T_{yy}. (b) Colored plot graphs of amplitudes, corresponding to the Fig. S2(a). (c) Transmitted amplitude and phase values described with line graph according to the square lengths.

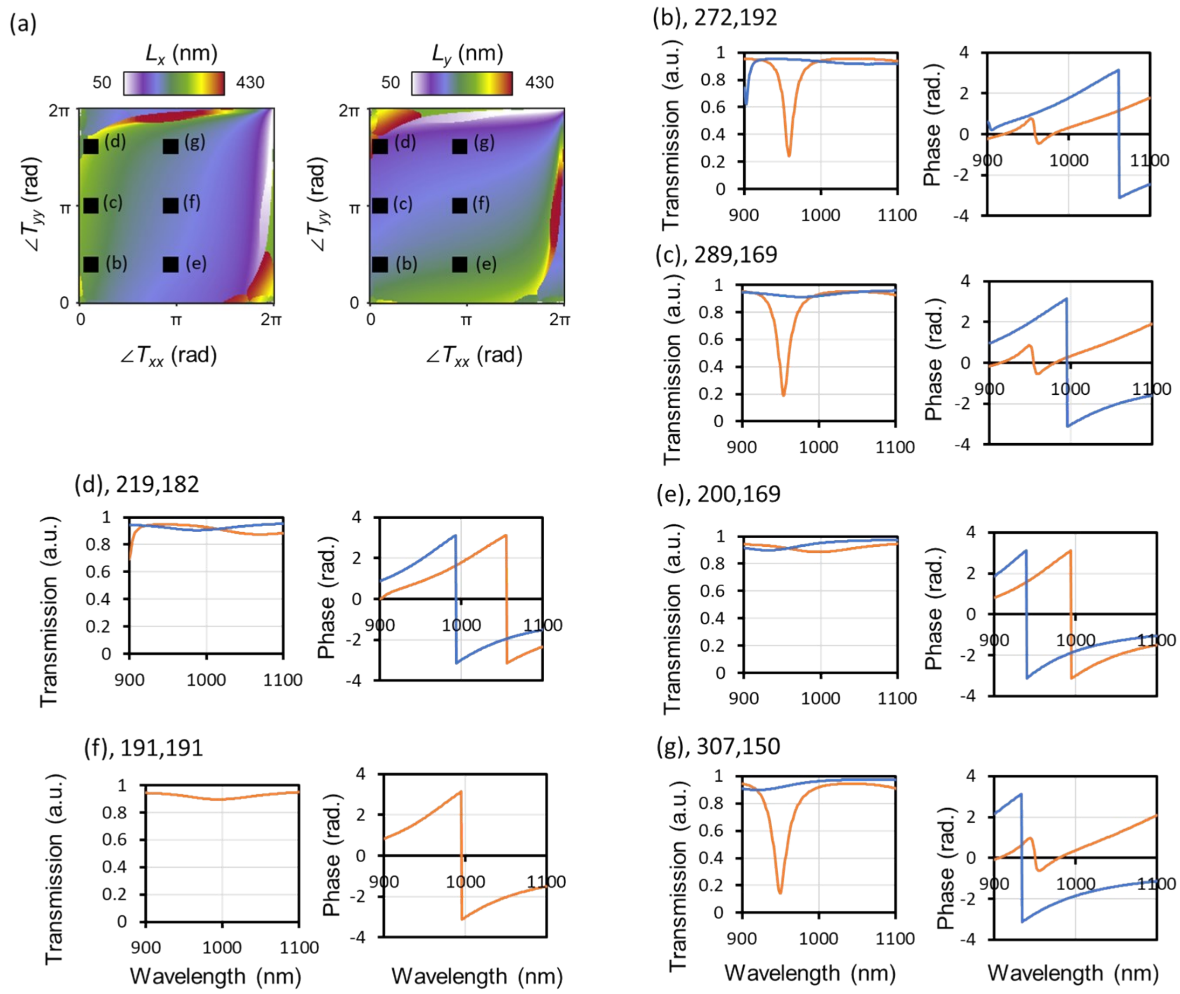

Figure S3. Dispersive characteristic of single nanopillars obtained from COMSOL Multiphysics. The wavelength bandwidth is from 900 to 1100 nm. (a) Colored plot graph relegated from Fig. S2. The square dot indicates the chosen structural parameters to be analyzed. (b-g) Chosen six structural nanopillars and their transmission amplitudes and phase values. The number values next to the alphabet means the value of L_x and L_y. Red line indicates information from T_{xx} and blue line from T_{yy}. The left graphs show transmission amplitude and the right is phase values. Since the structure (f) is isotropic, only information from T_{xx} is shown.

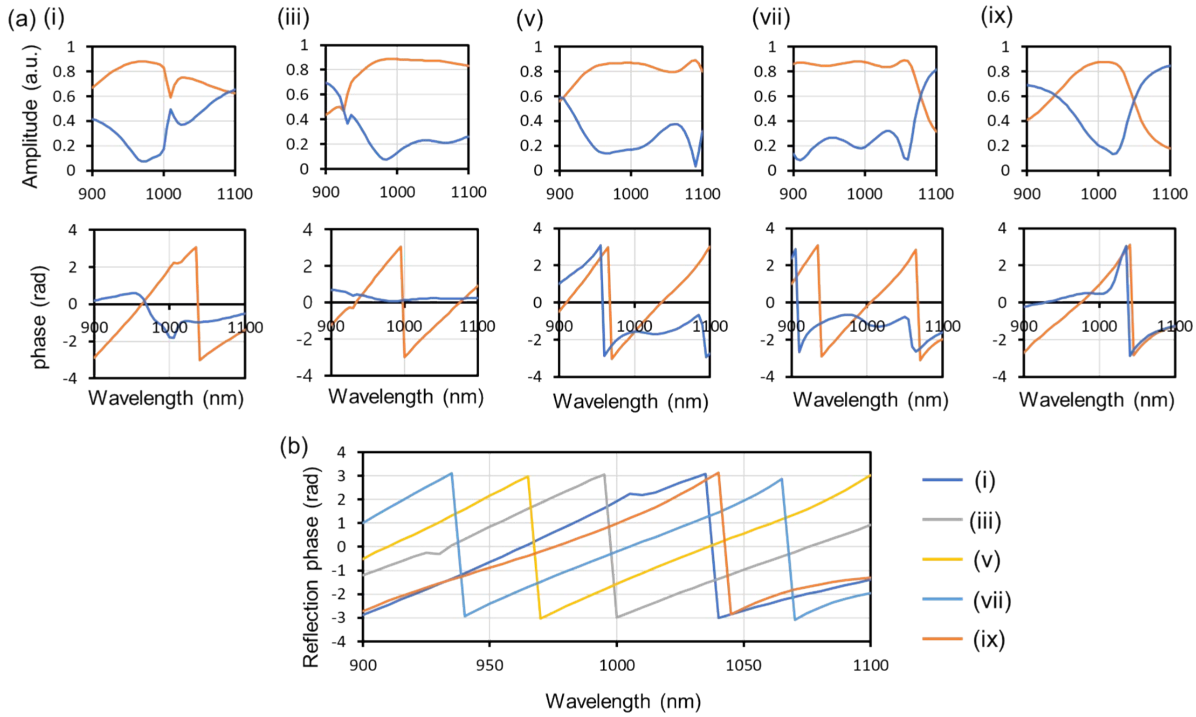

Figure S4. Dispersive characteristics of selected five parameters from Fig. 3 in the main text. (a) Upper graphs show the spectral characteristics transmission and reflection amplitudes and lower plot graphs show the phase values of (i), (iii), (v), (vii), (ix). Red lines are information from reflection and blues are from transmission. (b) Reflective phase values changing by the input wavelength. As shown in the graph, the difference does not persist for all wavelengths.

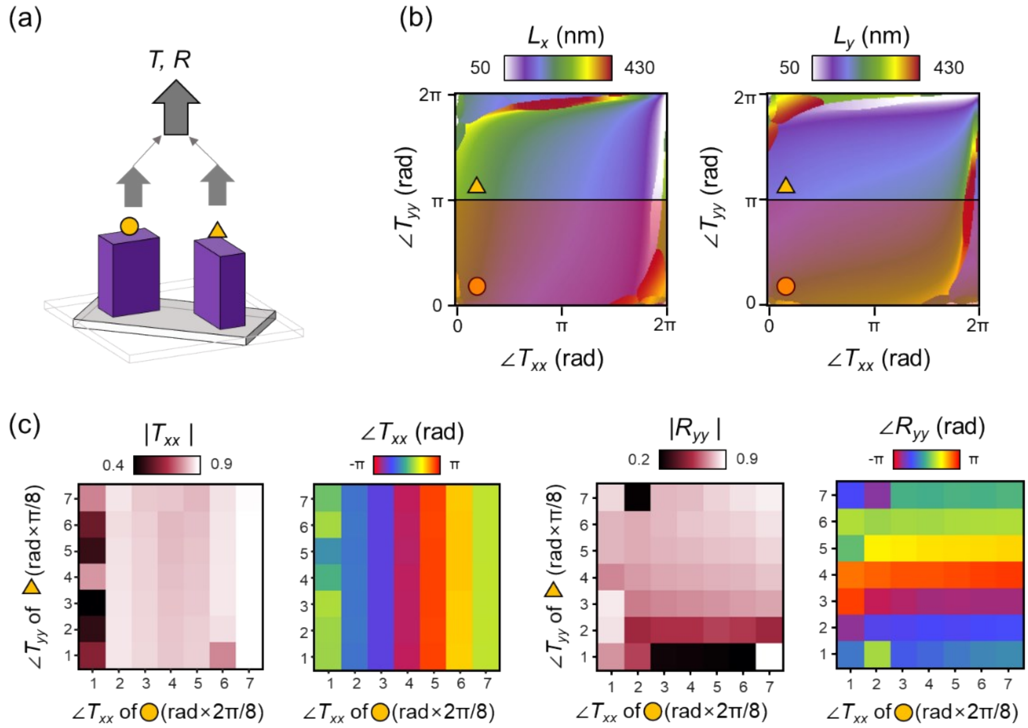

Figure S5. Schematic diagram and colored plot graphs for explanation of reflected phase values designed in linear polarization pair to operate like PBS, obtained by the scheme in the main text. (a) Schematic diagram of two-fold meta-atom unit cell design, and scattered wavefronts from each meta-atom is marked by yellow-colored circle and triangle, respectively. (b) Examples of structural parameters of two meta-atoms exhibiting transmission at *x*-polarized shined condition, and reflection at *y*-polarized shining. As mentioned in the main text, they should meet the condition of out-of-phase condition at T_{yy}, while T_{xx}s are in-phase. As results, line that passes circle and triangle both is parallel to y-axis. Note that the yellow circle can only be displaced in the red-shaded area, which is for evading the overlapped parameter set. That is in fact related to the reflected phase as mentioned in the main text: Reflected phase of R_{yy} is determined by the two times of T_{yy} of circle and triangle. (c) Determined phase and amplitude values of T_{xx} and R_{yy} extracted from resultant two-fold meta-atom, calculated by simulation. As shown in the graphs, it is noteworthy mentioning that the scale of y-axis is half of the scale in x-axis. At the same time, the phase values of T_{xx} and R_{yy} are changing with identical gradients, which means that the phase of R_{yy} changes two times faster than that of T_{xx}. And this result, as is repeatably noted here and the main text, is applied to various applications.

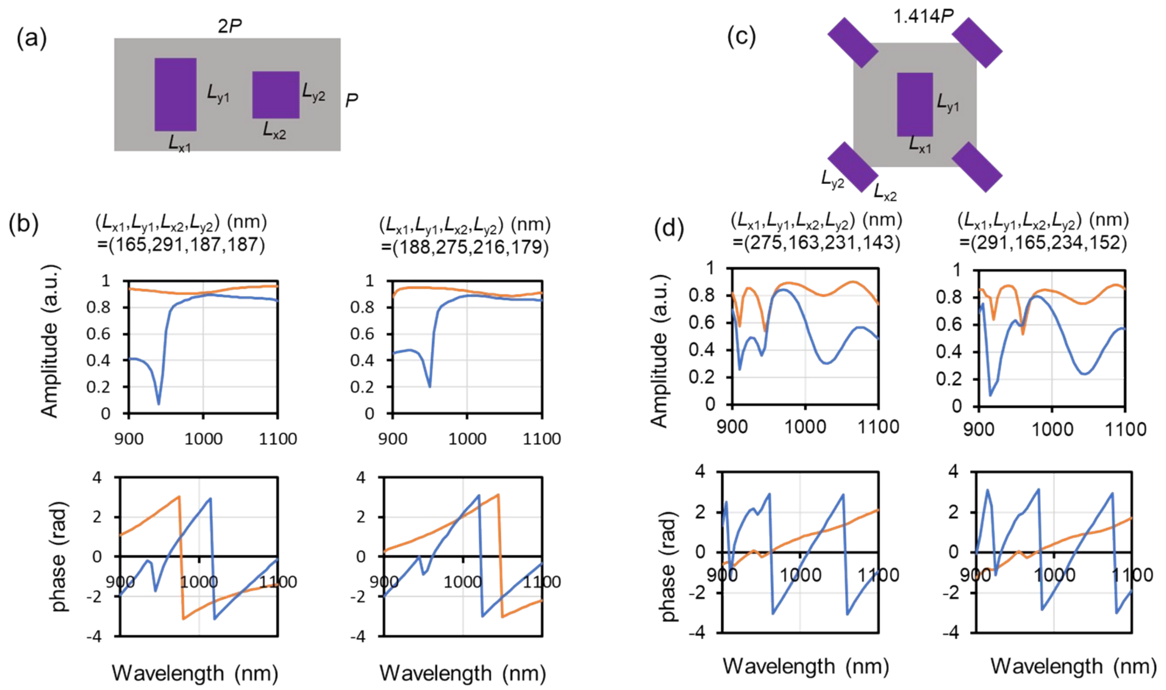

Figure S6. Dispersive characteristics of four selected parameters operating in full-space altered by input polarization (a) Schematic diagram for simulation space and structural parameter information for linear polarization basis structure. (b) Line plot graph of spectral distribution of amplitude (upper) and phase (lower) of transmission (T_{xx}, red line) and reflection (R_{yy}, blue line), calculated with parameters noted above graphs. R_{yy} is reflected y-polarized light when y-polarized light is incident. (c) Schematic diagram for simulation space and structural parameter information for circular polarization basis structure. (d) Line plot graph of spectral distribution of amplitude (upper) and phase (lower) of transmission (T_{lr}, red line) and reflection (R_{ll}, blue line), calculated with parameters noted above graphs. Subscripts l and r denotes the left-handed and right-handed circular polarization.

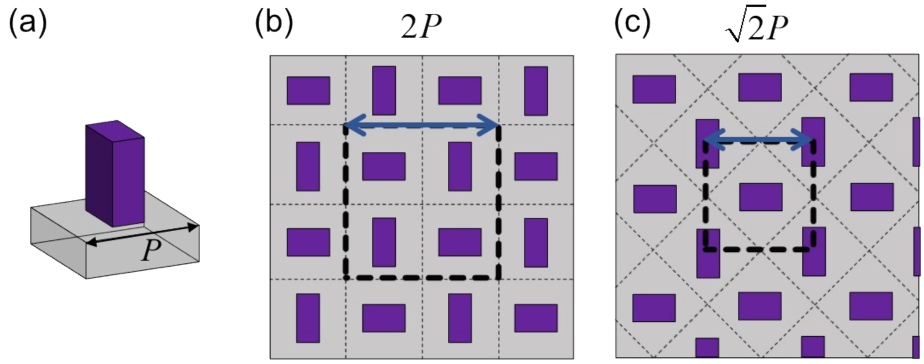

Figure S7. Pixel pitch difference by arrangement of meta-atoms in unit cell. (a) Schematic diagram of single meta-atom used in the main text. (b) Arrangement of four-fold meta-atoms which can be considered in intuitive manner. For fulfillment of square period with two interleaved meta-atoms, this structure gives pixel pitch of 2P as shown in the figure. (c) 45 degrees-inclined arrangement of two-fold meta-atom. This arrangement gives pixel pitch of $\sqrt{2}$ P, which provides denser information density compared to former case.

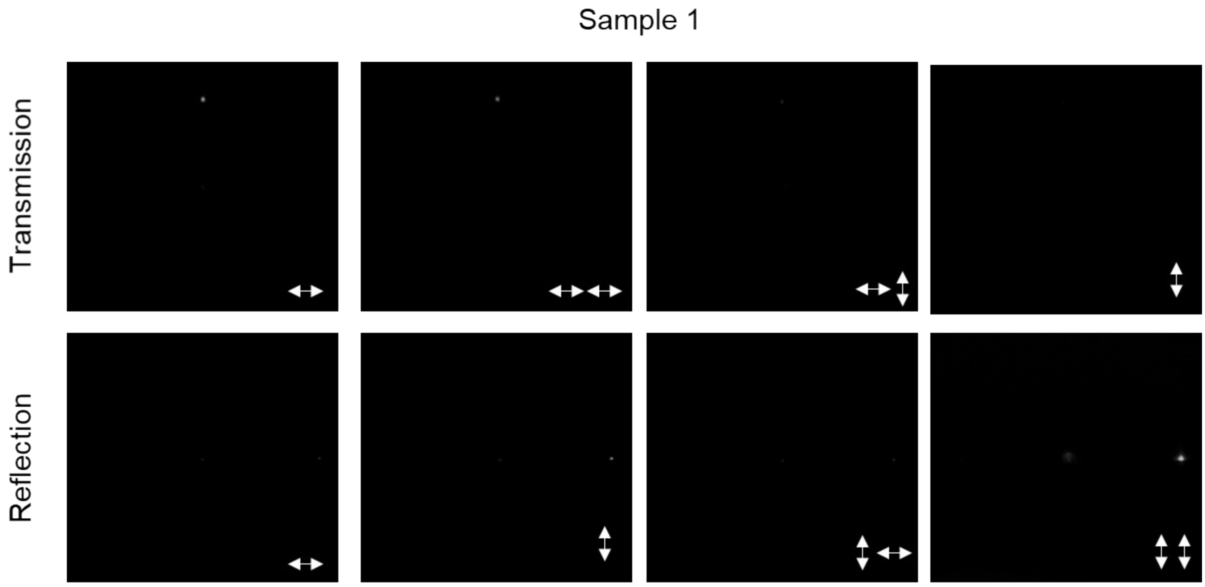

Figure S8. Experimental result measured from fabricated sample 1 operating in linear polarization pair. Captured images from upper row are from transmission spaces, and lower from reflection spaces. Arrows at lower right are basically the polarization state of input light, but when there are two arrows, each of them means the polarization state of input and output light.

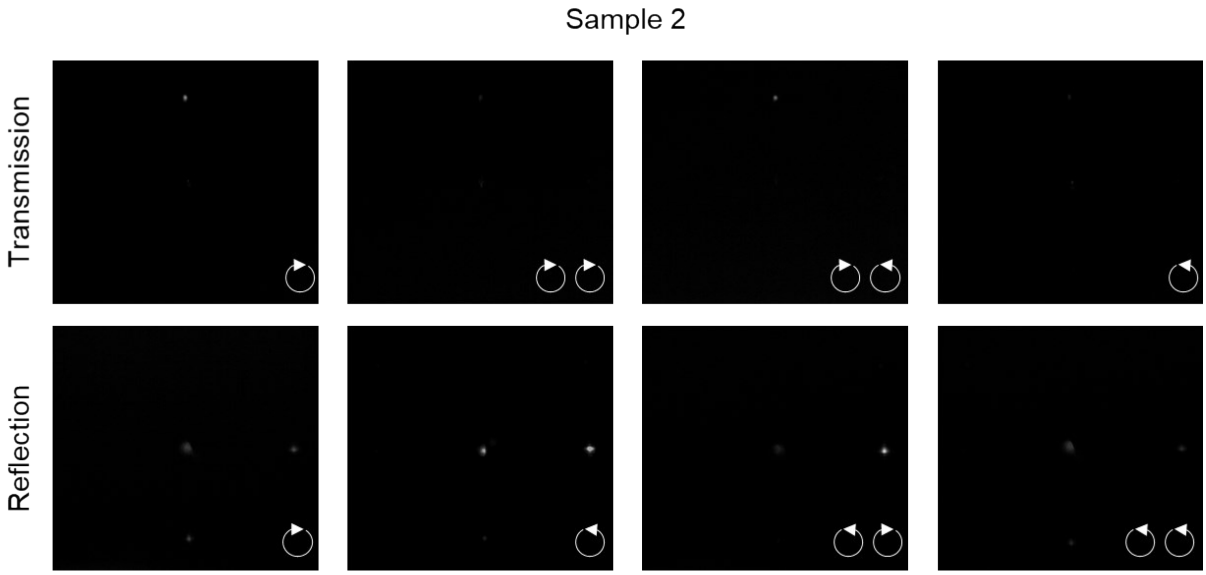

Figure S9. Experimental result measured from fabricated sample 2 operating in circular polarization pair. Captured images from upper row are from transmission spaces, and lower from reflection spaces. Arrows at lower right are basically the polarization state of input light, but when there are two arrows, each of them means the polarization state of input and output light.

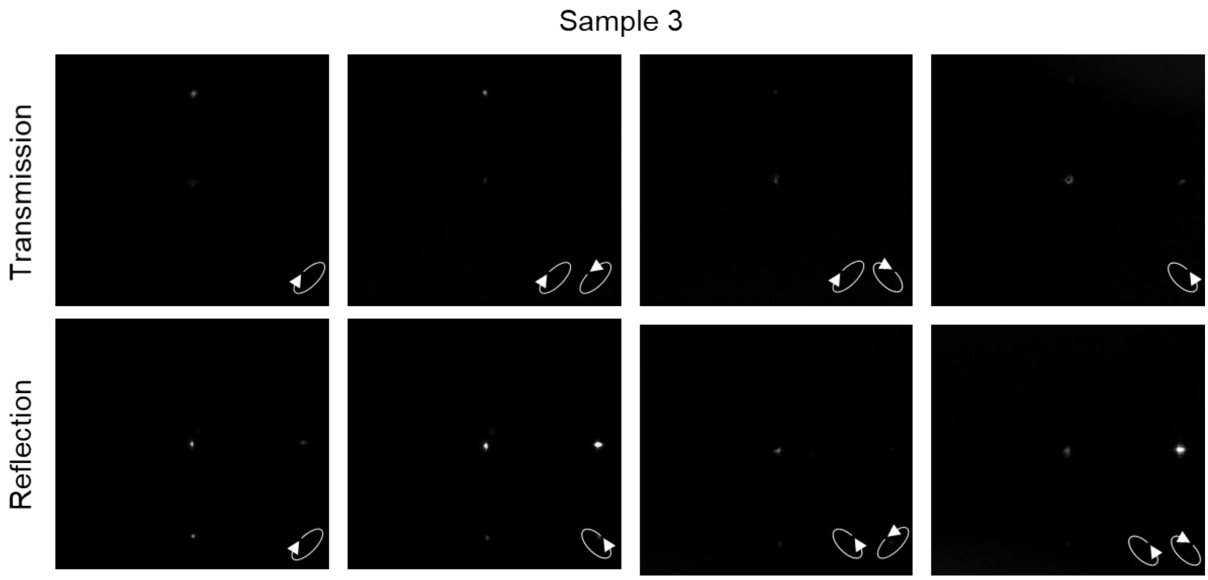

Figure S10. Experimental result measured from fabricated sample 3 operating in elliptical polarization pair. Captured images from upper row are from transmission spaces, and lower from reflection spaces. Arrows at lower right are basically the polarization state of input light, but when there are two arrows, each of them means the polarization state of input and output light.

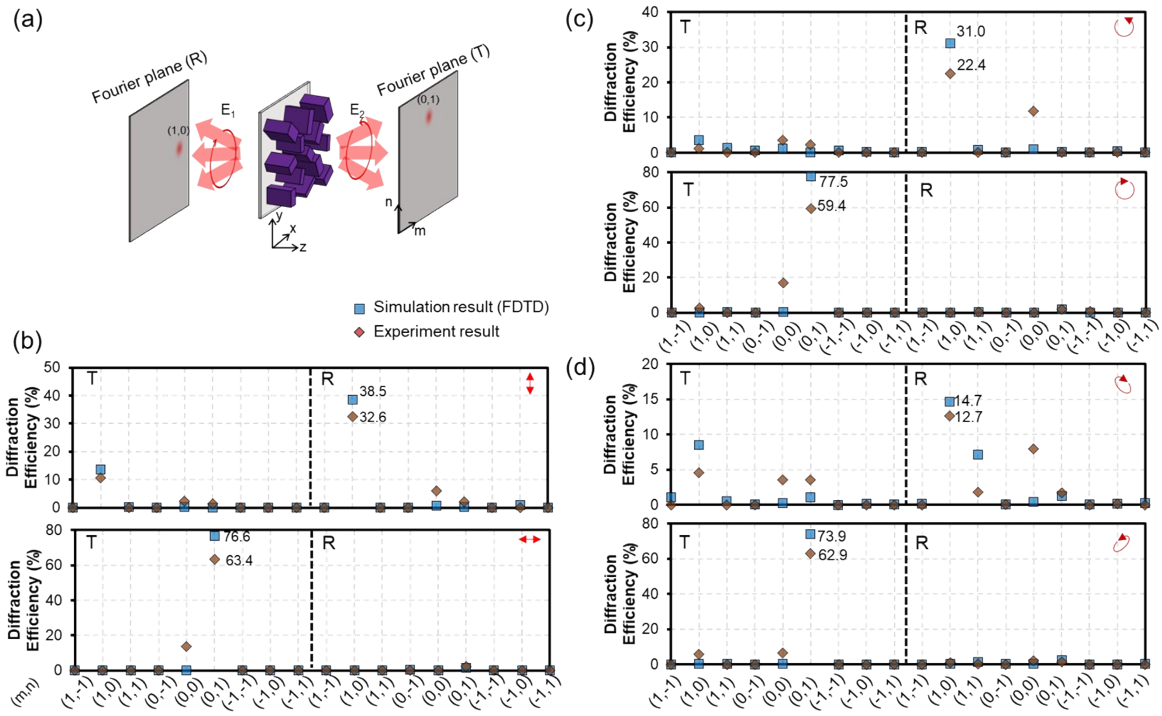

Figure S11. Beam deflection schematic diagram and results from simulation and experiment. (a) Schematic diagram showing beam deflection with parameters for diffraction order and polarization states. (b-d) Dot plot showing simulation and experiment result of diffraction order efficiency. (b) is from sample 1, operating in linear polarization pair, (c) from sample 2 operating in circular polarization pair and (d) from sample 3 operating in elliptical polarization pair. Arrows indicate the polarization states of the input light. The written numbers in graph are the diffraction efficiency of desired components. Blue squares are the simulated results and red diamonds are from measured results.

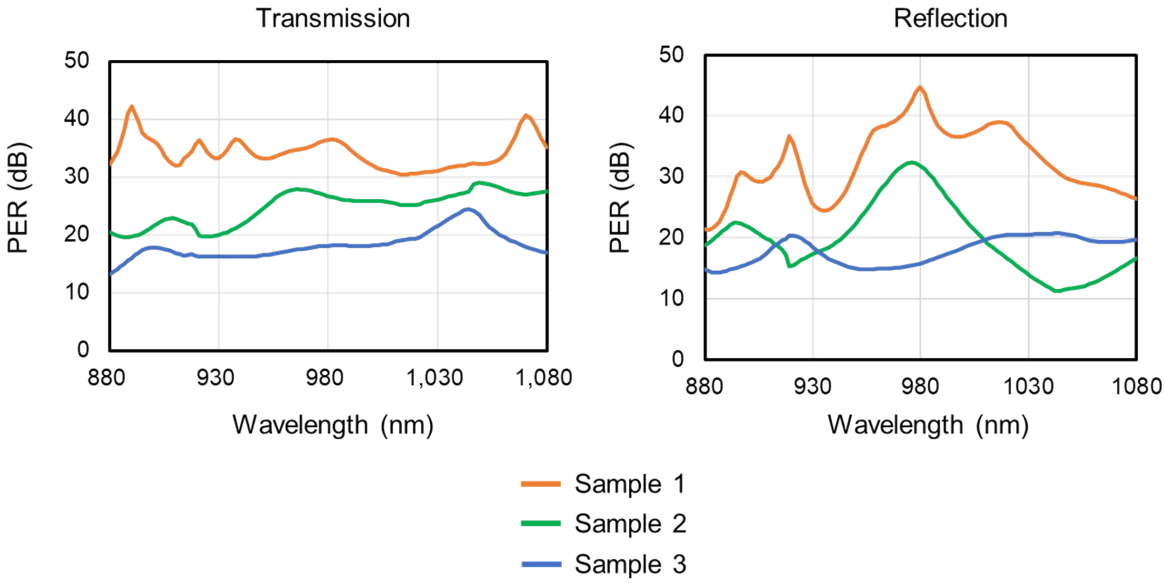

Figure S12. Dispersive characteristics of PER of the beam deflection samples in the main text.

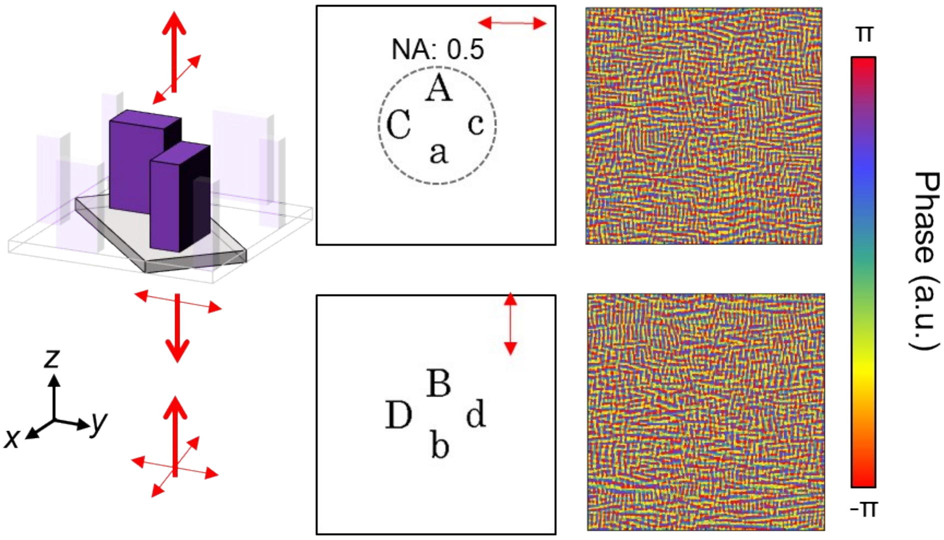

Figure S13. Conceptual diagram of linearly polarized light sample for how the holographic images are recorded into both spaces altered to be displayed by input polarization. As the maximal value of numerical aperture (NA) is 0.5, the holographic images are recorded considering that value. As a result, the letters in image occupies the area of narrower than the grey dotted circle, as shown in the graphs. The rightmost two images indicates the corresponed phase distributed values of corresponded image next to them. The other images are also calculated same, which is GS algorithm, as seen in the main text.

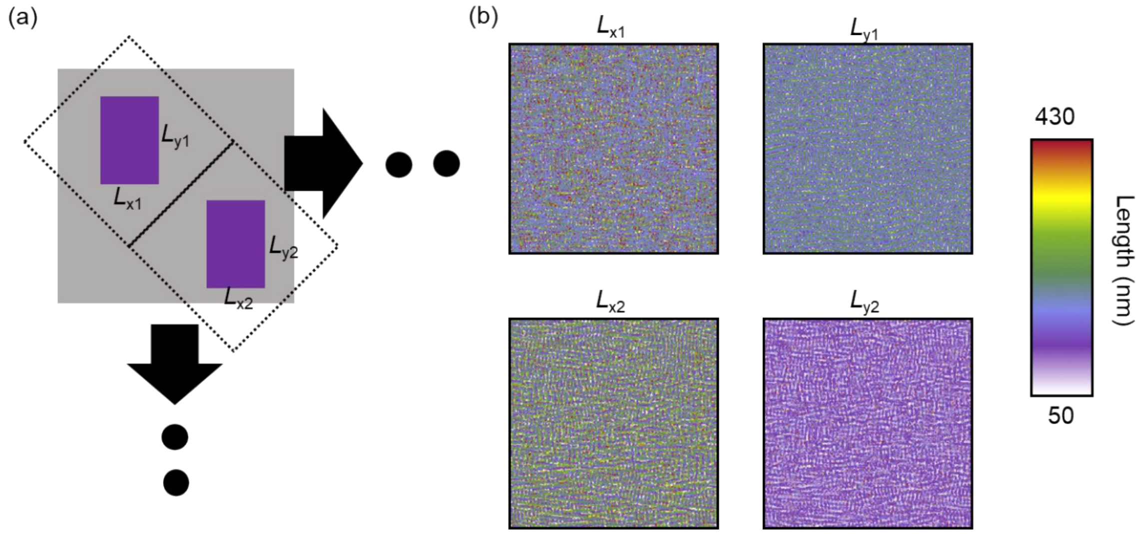

Figure S14. Structural parametric information of sample 1 at hologram generation sample. Since one unit consists of two nanopillars, the total number of nanopillars is 300×300×2. (a) The leftmost schematic shows how the nanopillars are arrranged and structural parameters are termed. (b) Length information. Each colored pixel shows the structural parameters for desired hologram generation.

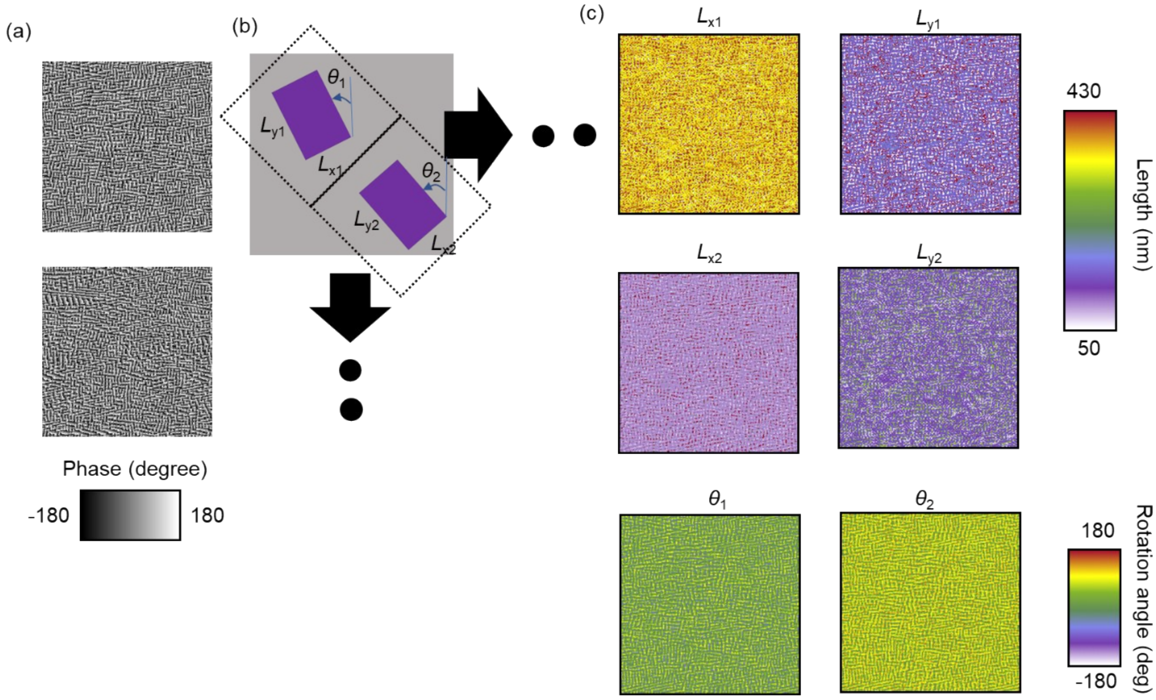

Figure S15. Structural parametric information of sample 2 at hologram generation sample. (a) The phase information for generation of desired hologram as shown in the main text. (b) Schematics showing how the nanopillars are arrranged and structural parameters are termed. (c) Length information. Each colored pixel shows the structural parameters for desired hologram generation.

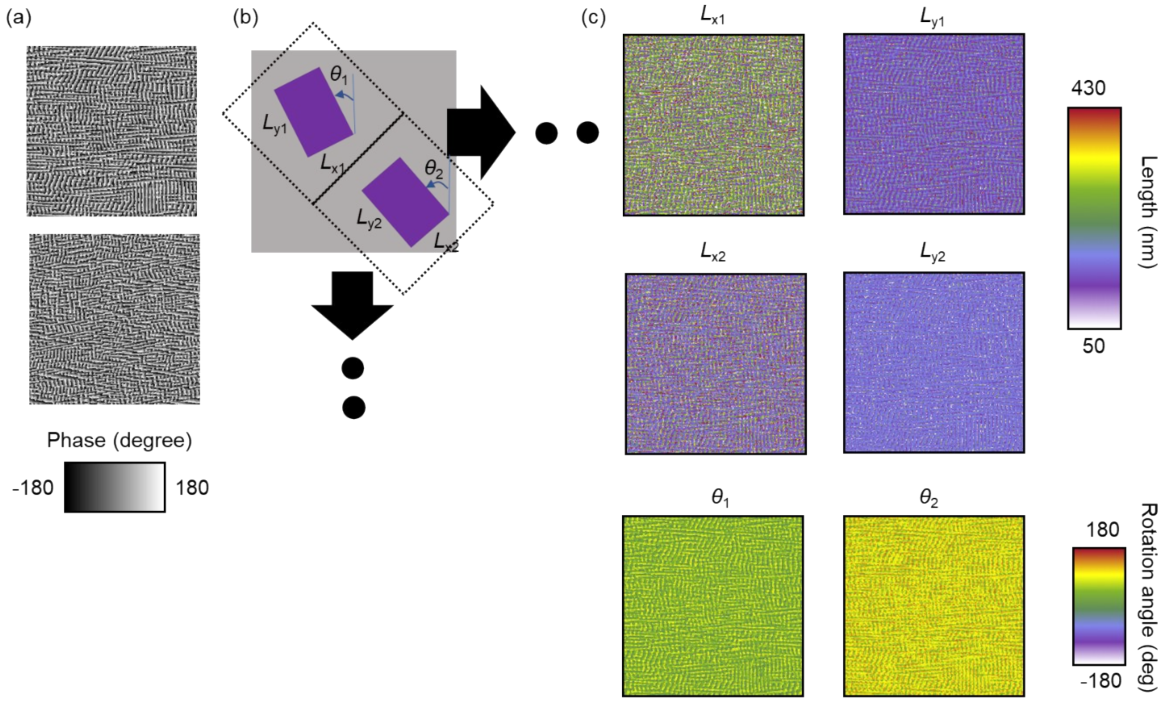

Figure S16. Structural parametric information of sample 3 at hologram generation sample. (a) The phase information for generation of desired hologram as shown in the main text. (b) Schematics showing how the nanopillars are arrranged and structural parameters are termed. (c) Length information. Each colored pixel shows the structural parameters for desired hologram generation.

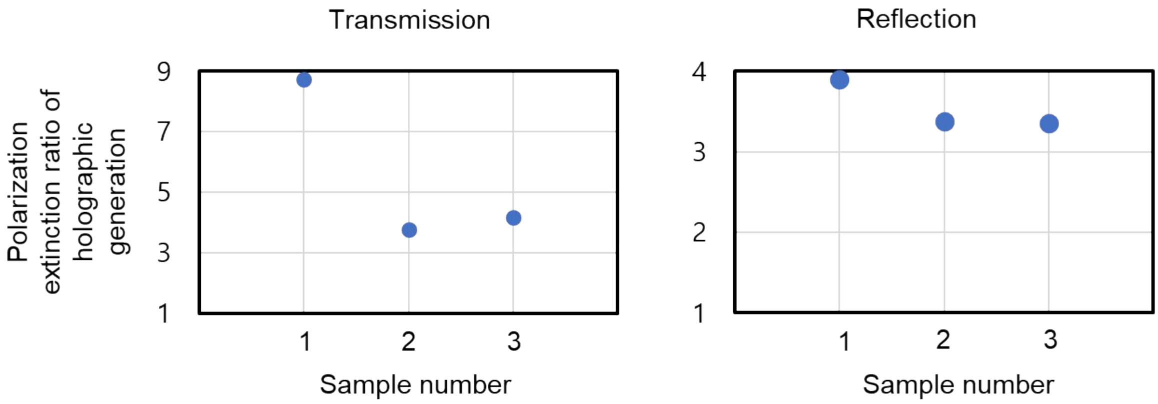

Figure S17. Polarization extinction ratio of hologram generation sample.

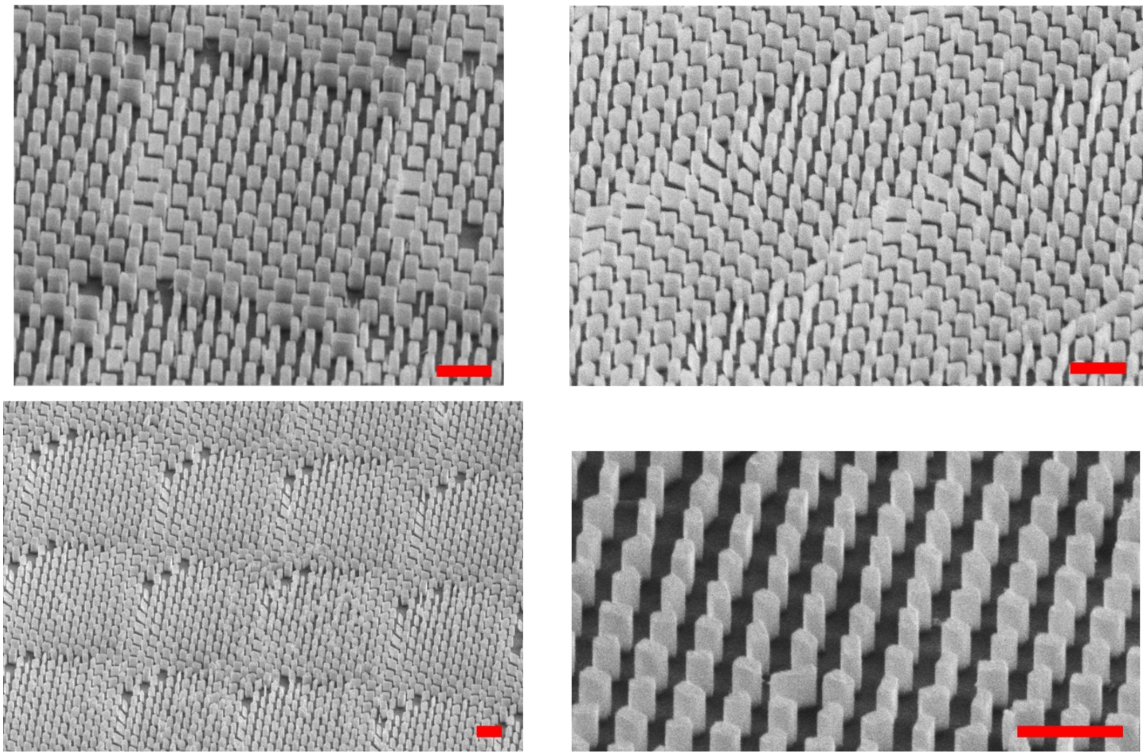

Figure S18. SEM-captured images from fabricated samples with various magnifications. (Upper left) Beam deflection sample 1 (Upper right) Beam deflection sample 2 (Lower left) Beam deflection sample 3 (Lower right) Hologram generation sample 2. Scale bar: 1 μm

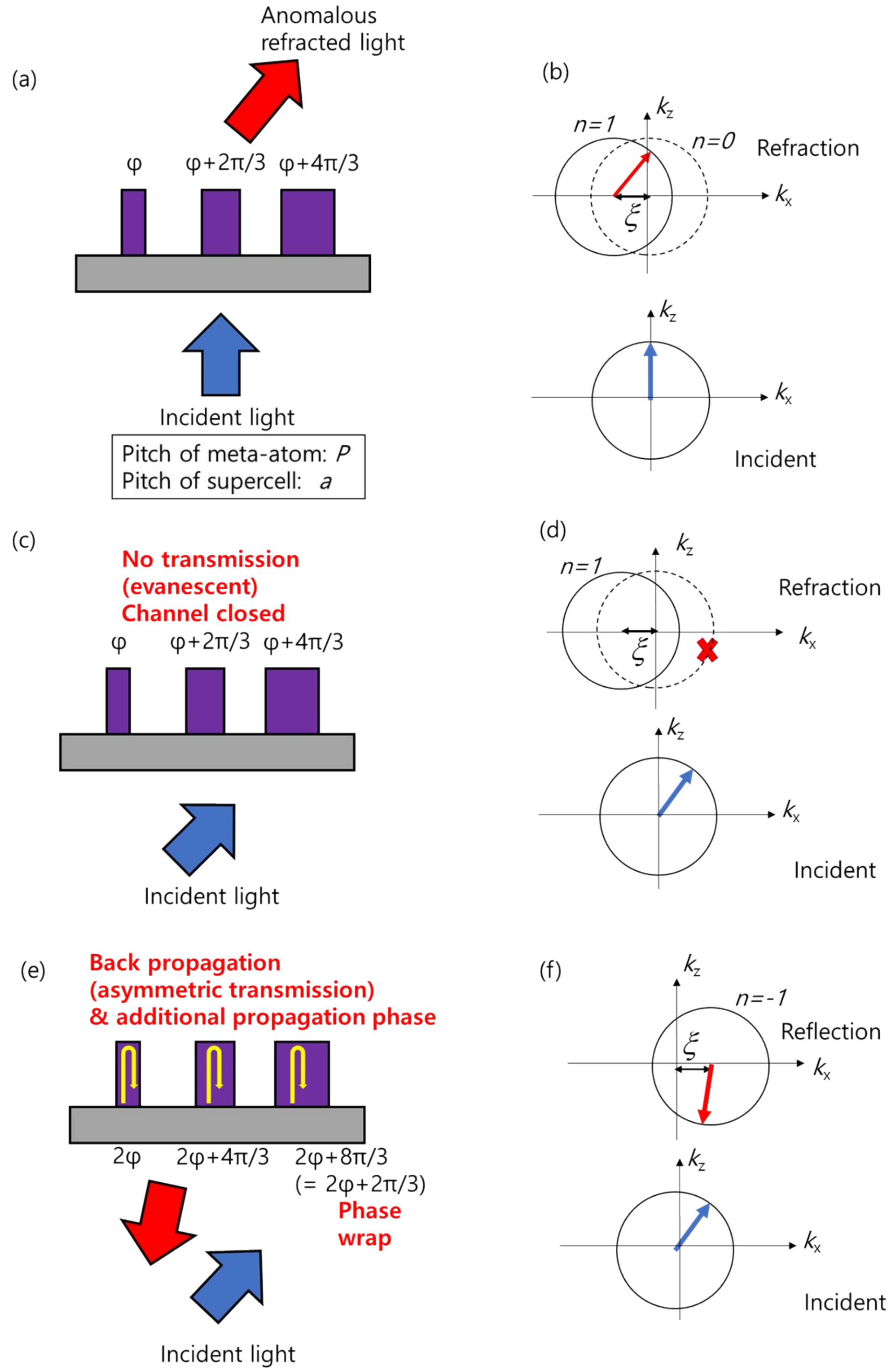

Figure S19. Procedure of how diffraction occurs when critical angle condition is met. (a) The condition when the diffraction can be explained with GSL. The transmitted phase values are noted on the nanopillars and this phase values show the phase gradient of ξ ($=2\pi/a=2\pi/3P$) into $+x$ direction. (b) Equifrequency contour. From bottom, the light is normally illuminating to structure, yielding anomalous refraction. The solid circle at the bottom (Incident) represents the isofrequency contour of incident light. Blue arrow shows the direction of incident light, and red arrow at the upper graph (Refraction) represents the propagating direction of refracted light. The dashed circle in refraction is the contour for reference when there is no phase gradient by the structure. On the other hand, the solid circle is the shifted contour by phase gradient ξ, order of n=1 (by GSL). As shown by the direction of red arrow, the propagating direction of refraction can be accesssed. (c) Schematic of obliquely incident light when critical angle condition is met. By GSL, the refracted light cannot exist, because the momentum becomes bigger than the free space wavenumber k0. (d) Equifrequency contour described by GSL. One can find that using the same scheme to decide the refracted light by the Fig. S19b cannot determine the light trajectory diffracted by this structure. (e) Schematic diagram showing the induced reflection mentioned in the main text. As the refraction by GSL is not possible, the wave propagates back into reflection space, yielding two times of propagation phase. This, in turn, results in the diffraction having order of n=-1, which follows the equation (5) in the main text. The diffraction order n can be obtained using equation (5), so rather than GSL, diffraction law of parity reversal (equation (4) in the main text) should be utilized in critical angle condition. (f) Corresponded equifrequency contour. The transverse shift of solid circle is determined by the equation (5) as mentioned above, and the light propagating direction can be retrieved by this.

Table S1. Widths of square nanopillars shown in Fig. 3a.

Set		(i)	(ii)	(iii)	(iv)	(v)	(vi)	(vii)	(viii)	(ix)	(x)
Width [nm]	Left	187	184	181	178	174	169	163	154	141	115
	Right	279	238	228	218	210	205	200	197	194	190

Table S2. Structural parametric information of beam steering sample 1. The notation of parameter is same as Fig. S14

Parameter	Length (nm)							
L_{x1}	50	333	358	268	275	279	284	287
	203	224	230	236	241	246	249	254
	196	200	205	210	214	217	220	223
	182	186	191	195	198	201	204	207
	173	176	181	185	188	191	193	195
	165	168	172	176	179	181	183	186
	156	159	163	167	170	172	174	176
	146	149	153	156	159	161	163	165
	417	133	136	140	143	145	147	149
	268	424	142	142	143	146	148	150
L_{y1}	50	214	196	198	188	181	175	170
	348	240	220	205	195	187	181	175
	269	250	229	213	202	194	188	182
	279	258	235	219	208	199	192	186
	285	265	241	224	212	203	196	190
	291	271	247	229	216	207	200	193
	301	280	254	234	221	212	204	197
	312	289	263	243	228	218	210	203
	242	311	284	259	241	230	220	212
	247	203	188	339	299	276	258	245
L_{x2}	291	296	303	312	239	243	50	261
	257	261	266	271	282	299	344	196
	227	229	233	239	245	258	292	175
	209	212	215	218	224	234	257	426
	197	199	202	205	211	219	236	430
	187	189	192	195	199	206	221	427
	178	180	182	185	189	195	207	256
	167	169	171	173	177	182	193	229
	151	152	154	157	160	164	173	199
	117	119	121	123	126	129	136	154
L_{y2}	165	160	154	147	424	413	249	327
	170	165	159	153	144	132	111	402
	176	171	165	158	150	138	117	430
	181	175	169	163	154	142	122	79
	184	179	173	166	157	145	126	72
	188	182	176	169	160	148	129	64
	191	185	179	172	163	151	132	92

	196	189	183	176	166	154	135	96
	204	198	191	182	173	160	140	102
	233	223	213	203	191	176	154	113

Table S3. Structural parametric information of beam steering sample 2. The notation of parameter is same as Fig. S15

Parameter	Length (nm) or Angle (degree)							
L_{x1}	256	247	241	237	234	232	231	234
	249	243	237	234	232	231	233	238
	243	239	234	232	231	232	237	249
	239	235	232	231	232	236	245	273
	235	232	232	232	234	242	264	427
	234	232	231	234	241	257	430	430
	232	231	233	238	252	428	429	165
	231	232	237	249	430	430	165	164
	232	236	245	273	430	165	164	163
	234	242	264	427	429	164	163	162
L_{y1}	161	160	158	155	152	148	143	135
	160	158	156	153	149	144	137	128
	159	156	154	150	145	139	130	117
	157	154	151	146	140	132	120	101
	155	152	147	141	134	123	106	69
	152	148	143	135	125	110	69	66
	149	144	137	128	114	70	67	293
	145	139	130	117	70	67	295	288
	140	132	120	101	68	297	290	282
	134	123	106	69	66	292	284	275
L_{x2}	241	257	430	430	165	163	163	162
	252	428	429	165	164	163	162	161
	430	430	165	164	163	162	161	160
	430	165	164	163	162	161	160	159
	429	164	163	162	162	161	159	157
	165	163	163	162	161	160	158	155
	164	163	162	161	160	158	156	153
	163	162	161	160	159	156	154	150
	162	161	160	159	157	154	151	146
	162	161	159	157	155	152	147	141
L_{y2}	125	110	69	66	291	286	275	265
	114	70	67	293	286	277	267	258
	70	67	295	288	279	270	260	251
	68	297	290	282	272	263	253	245
	66	292	284	275	263	253	247	241
	291	286	275	265	256	247	241	237
	286	277	267	258	249	243	237	234

	279	270	260	251	243	239	234	232
	272	263	253	245	239	235	232	231
	263	253	247	241	235	232	232	232
θ_1	22.5	28.125	33.75	39.375	45	50.625	56.25	61.875
	9	14.625	20.25	25.875	31.5	37.125	42.75	48.375
	-4.5	1.125	6.75	12.375	18	23.625	29.25	34.875
	-18	-12.375	-6.75	-1.125	4.5	10.125	15.75	21.375
	-31.5	-25.875	-20.25	-14.625	-9	-3.375	2.25	7.875
	-45	-39.375	-33.75	-28.125	-22.5	-16.875	-11.25	-5.625
	-58.5	-52.875	-47.25	-41.625	-36	-30.375	-24.75	-19.125
	-72	-66.375	-60.75	-55.125	-49.5	-43.875	-38.25	-32.625
	-85.5	-79.875	-74.25	-68.625	-63	-57.375	-51.75	-46.125
	-99	-93.375	-87.75	-82.125	-76.5	-70.875	-65.25	-59.625
θ_2	67.5	73.125	78.75	84.375	90	95.625	101.25	106.875
	54	59.625	65.25	70.875	76.5	82.125	87.75	93.375
	40.5	46.125	51.75	57.375	63	68.625	74.25	79.875
	27	32.625	38.25	43.875	49.5	55.125	60.75	66.375
	13.5	19.125	24.75	30.375	36	41.625	47.25	52.875
	0	5.625	11.25	16.875	22.5	28.125	33.75	39.375
	-13.5	-7.875	-2.25	3.375	9	14.625	20.25	25.875
	-27	-21.375	-15.75	-10.125	-4.5	1.125	6.75	12.375
	-40.5	-34.875	-29.25	-23.625	-18	-12.375	-6.75	-1.125
	-54	-48.375	-42.75	-37.125	-31.5	-25.875	-20.25	-14.625

Table S4. Structural parametric information of beam steering sample 3. The notation of parameter is same as Fig. S15

Parameter	Length (nm) or Angle (degree)							
L_{x1}	239	319	310	303	292	279	267	253
	315	317	324	341	380	172	184	179
	299	321	378	176	173	187	183	180
	283	348	172	188	186	185	183	182
	262	418	182	182	182	183	182	182
	241	429	174	176	178	180	180	180
	226	429	167	170	173	175	176	177
	218	281	159	161	165	169	171	171
	222	397	150	152	156	159	162	164
	268	424	142	142	143	146	148	150
L_{y1}	424	135	132	128	125	123	122	123
	133	126	117	106	93	430	285	287
	128	114	95	428	422	275	272	268
	123	98	430	277	270	261	253	245
	122	81	283	273	260	246	238	229
	125	74	286	270	252	237	228	221
	127	66	290	269	249	234	224	216
	124	84	297	278	253	234	222	215
	111	53	305	286	260	241	226	217
	76	244	307	292	272	251	237	226
L_{x2}	125	127	127	124	119	108	89	50
	290	293	63	57	51	310	313	313
	265	265	268	272	275	280	286	292
	239	237	235	237	239	245	252	263
	225	222	220	219	220	223	229	239
	216	213	211	210	210	211	214	223
	212	208	206	204	204	204	207	212
	210	206	203	202	200	200	202	207
	211	206	203	200	199	199	201	206
	217	211	207	203	202	202	206	218
L_{y2}	125	110	69	66	291	286	275	265
	114	70	67	293	286	277	267	258
	70	67	295	288	279	270	260	251
	68	297	290	282	272	263	253	245
	66	292	284	275	263	253	247	241
	291	286	275	265	256	247	241	237
	286	277	267	258	249	243	237	234

	279	270	260	251	243	239	234	232
	272	263	253	245	239	235	232	231
	263	253	247	241	235	232	232	232
θ_1	0	5.625	11.25	16.875	22.5	28.125	33.75	39.375
	-9	-3.375	2.25	7.875	13.5	19.125	24.75	30.375
	-18	-12.375	-6.75	-1.125	4.5	10.125	15.75	21.375
	-27	-21.375	-15.75	-10.125	-4.5	1.125	6.75	12.375
	-36	-30.375	-24.75	-19.125	-13.5	-7.875	-2.25	3.375
	-45	-39.375	-33.75	-28.125	-22.5	-16.875	-11.25	-5.625
	-54	-48.375	-42.75	-37.125	-31.5	-25.875	-20.25	-14.625
	-63	-57.375	-51.75	-46.125	-40.5	-34.875	-29.25	-23.625
	-72	-66.375	-60.75	-55.125	-49.5	-43.875	-38.25	-32.625
	-81	-75.375	-69.75	-64.125	-58.5	-52.875	-47.25	-41.625
θ_2	45	50.625	56.25	61.875	67.5	73.125	78.75	84.375
	36	41.625	47.25	52.875	58.5	64.125	69.75	75.375
	27	32.625	38.25	43.875	49.5	55.125	60.75	66.375
	18	23.625	29.25	34.875	40.5	46.125	51.75	57.375
	9	14.625	20.25	25.875	31.5	37.125	42.75	48.375
	0	5.625	11.25	16.875	22.5	28.125	33.75	39.375
	-9	-3.375	2.25	7.875	13.5	19.125	24.75	30.375
	-18	-12.375	-6.75	-1.125	4.5	10.125	15.75	21.375
	-27	-21.375	-15.75	-10.125	-4.5	1.125	6.75	12.375
	-36	-30.375	-24.75	-19.125	-13.5	-7.875	-2.25	3.375